Adhesion of Polycarbonate Blends on a Nickel Surface

Denis Andrienko,*,† Salvador León,‡ Luigi Delle Site,† and Kurt Kremer†

*Max-Planck-Institut für Polymerforschung, Ackermannweg 10, 55128 Mainz, Germany,
Department of Chemical Engineering, ETSII/UPM, Jose Gutierrez Abascal 2, 28006 Madrid, Spain*

ABSTRACT: We demonstrate that the adhesive behavior of a phenol-terminated bisphenol A polycarbonate melt to a (111) nickel surface changes significantly if a small amount of short chains is present, i.e., in polydispersed melts or self-blends. Attractive interaction of the chain ends with the surface results in an adsorbed layer, made of single- and two-end attached chains. Short chains, however, diffuse from the bulk and occupy the adsorption sites much faster than the long ones. Interplay between the surface concentration of short chains, their molecular conformation, and excluded volume results in a nonmonotonic dependence of the surface coverage by long chains on the molecular weight of the additive. The smallest polycarbonate coverage is achieved for diphenyl carbonate due to its high mobility and relatively large excluded volume. We propose that self-blending can be used to modify, in a controlled fashion, the friction coefficient of a melt sheared past the nickel surface.

I. Introduction

Bisphenol A polycarbonate (BPA-PC) is by far the most utilized and, therefore, intensively studied variety of polycarbonates.[1] The combination of high impact strength, ductility, high glass transition and melting temperatures, and good mechanical and optical properties makes it an ideal material for compact disks, automotive components, and ophthalmic applications.[2] It has also become an attractive test system for the coarse-graining techniques,[3–7] which are vital for calculation of macroscopic properties without involving computationally expensive atomistic simulations.[8,9]

Industrial processing of polycarbonate melts includes its fast shearing past metal surfaces.[10] At this stage, adhesive properties of the melt are crucial for the quality of the final product. Packing of polymer chains close to the walls also poses a number of interesting scientific questions, e.g., how the interplay between the local adsorption energy of chain segments and conformational entropy of the chains influences the structure of the adsorbed layer.[11–14] In fact, this structure can now be studied at the atomic scale, thanks to developments of a variety of experimental techniques, the most well-known being atomic force microscopy, scanning tunneling microscopy, and surface force apparatus.[15,16] To link the results of the measurements with theory, it is necessary to predict the structure of the adsorbed layer at a microscopic (atomic) scale. At this level of description computer simulation techniques are proven to be useful for bridging between theory and experiment.

Indeed, extensive studies involving ab initio calculations,[17] atomistic simulations,[6] and various coarse-graining schemes[4,6] were employed to first reproduce the properties of the bulk and then to study adsorption on a nickel surface[18] of monodispersed BPA-PC melts. It was shown that a certain amount of chain ends becomes quasi-permanently bound to the surface. As a result, two distinct overlapping layers are formed by the single- and two-end adsorbed chains. The layer composed of the two-end adsorbed chains is made of entangled loops, with the configuration reflecting the statistics of the chains in the melt. The single-end adsorbed chains are stretched and form a brushlike layer interdigitated with the bulk of the melt.[6,7,17,18] It was also proposed that interdigitation and disentanglement of the adsorbed chains play a key role on the flow of polymer melt, in particular on the appearance of flow with slip at the wall.[19]

Polymerization of polycarbonates normally results in a polydispersed melt, with a small concentration of, for example, phenol or diphenyl carbonate ($\approx 0.1\%$ in weight). Moreover, to obtain more easily processed melts with enhanced flow properties, polymer self-blending is often used.[20] A controlled addition of the lower weight polymer improves the processability without sacrificing the mechanical properties of the high molecular weight material.

Although a small amount of additives does not affect the bulk properties of the melt, it can significantly change its adhesive behavior. Indeed, short and therefore more mobile molecules can quickly diffuse and adsorb on the walls, occupying the adsorption sites otherwise available for the high molecular weight component. A microscopically thin surface layer screens the interactions of the melt with the wall. As a result, those surfaces on which polymer melts normally adsorb (or brushes anchor) can become nonadsorbing, and the stick (no slip) boundary conditions for the flow of the melt near the wall can change to the hydrodynamic slip with a finite slip length.[21]

In this paper, as an initial step toward polydispersed systems, we study the adhesion behavior of bidispersed melts of BPA-PC on a (111) nickel surface. In particular, we would like to understand which additives provide the best screening of the interaction between the wall and the polymer melt.

The paper is organized as follows: we first recapitulate the dual resolution scheme used to coarse-grain BPA-PC and describe the simulation techniques in section II. Then, in section III, we study the structure of the adsorbed layer typical for monodispersed melts and compare the adhesive properties of monodispersed and bidispersed melts as well as the melts without

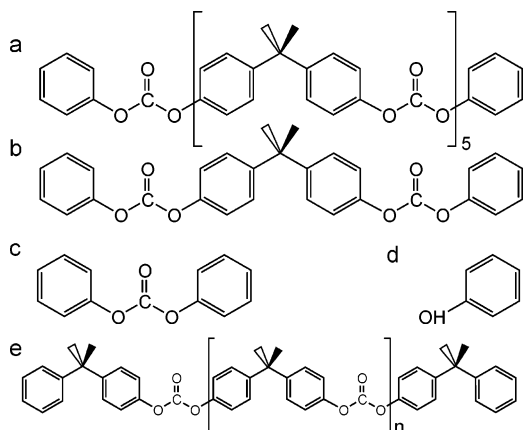† Max-Planck-Institut für Polymerforschung.
‡ ETSII/UPM.

Figure 1. Chemical structures of studied additives: (a) bisphenol A polycarbonate molecule of five repeat units; (b) one repeat unit BPA-PC; (c) diphenyl carbonate (DPC); (d) phenol; (e) chains with *p*-cumylphenolic (weakly adsorbing) chain ends.

Table 1. Studied Systems[a]

N_1, N_2	n_1, n_2	L_z, Å	chain ends
5	500	124	phenolic
20	240	214	phenolic
20, 5	240, 50	225	phenolic
20, 5	240, 50	225	phenolic, no adsorption
20, 5	240, 50	239	*p*-cumylphenolic
20, 5	240, 50	239	*p*-cumylphenolic (no adsorption)
20, 1	240, 143	225	phenolic
20, DPC	240, 312	224	phenolic
20, phenol	240, 711	211	phenolic

[a] In the case of mixtures, the major component is $N_1 = 20$ repeat units bisphenol A polycarbonate. The second component is either five repeat units BPA-PC, one repeat unit BPA-PC, diphenyl carbonate (DPC), or phenol. Note that the radius of gyration of the long chains (6.2σ or 27 Å) is always much smaller than the slit pore thickness, L_z.

strong adsorption of the chain ends to the surface. Finally, concluding remarks and a brief discussion of the implication of our work to the surface friction appear in section IV.

II. Simulation Details

A. Studied Systems. We study four types of polymer mixtures. The host polymer (major component) is comprised of the phenol-terminated BPA-PC chains of $N_1 = 20$ repeat units. The second (minor) component is one of the following: BPA-PC of $N_2 = 5$ repeat units, one repeat unit BPA-PC, diphenyl carbonate (DPC), or phenol. The corresponding chemical structures are depicted in Figure 1. To separate the effects due to the additives from the effects already present in monodipersed systems, we also studied two monodispersed polymer melts of $N_1 = 20$ and $N_1 = 5$ repeat units. Finally, for the 20:5 mixture we considered several possible types of the chain ends: phenolic (strongly adsorbing to the surface), *p*-cumylphenolic (weakly adsorbing to the surface), and phenolic and *p*-cumylphenolic without chain end attraction to the surface.

For all mixtures, we used $n_1 = 240$ chains of the major component of 20 repeat units. The number of the chains (or molecules) of the minor component was then adjusted to provide (approximately) 5% in weight of the total system. Exact numbers used in simulation are given in Table 1.

B. Coarse-Graining Scheme. We use the previously developed 4:1 coarse-graining model.[6] Briefly, each
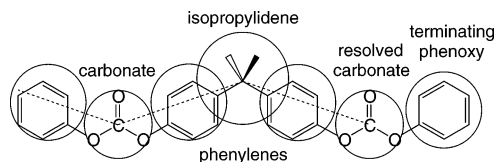

Figure 2. Dual-resolution coarse-graining scheme: isopropylidene, carbonate, and inner phenylenes are replaced by four beads. Terminating carbonates are resolved atomistically, so that the angular orientation of the terminating phenolic group is known.

Table 2. Coarse-Grained Bead Diameters in Lennard-Jones σ and Angstroms[a]

bead	σ	Å
carbonate	0.79	3.5
isopropylidene	1.18	5.2
phenylene	1.06	4.7

[a] Scaling factor is 4.41 Å/σ.

Table 3. Coarse-Grained Mean Bond Lengths[a]

beads	σ	Å
isopropylidene−phenylene	0.66	2.9
carbonate−phenylene	0.81	3.6

[a] Standard deviation $\delta l/\sigma = 0.02$. Scaling factor is 4.41 Å/σ.

monomer is replaced by four beads that correspond to isopropylidene, carbonate, and the two linking phenylenes, as shown in Figure 2. Bead sizes are computed by first calculating gyration radii of each group and then scaling them, such that the volume of the repeat unit, accounting for overlaps, is equal to the van der Waals volume per repeat unit computed from the equation-of-state analysis.[4] The mapping points for carbonate and isopropylidene are taken as backbone carbon atoms for each group, while the phenylenes lie in the straight line between the carbonate and isopropylidene. All beads interact via nonbonded repulsive Lennard-Jones potential and intramolecular bond angle and harmonic spring potentials. Each inner phenylene bead is connected by stiff harmonic bonds to its neighboring isopropylidene and carbonate. The lengths of these bonds ensure the proper isopropylidene−carbonate intramolecular distance. Bond parameters and bead sizes are given in Tables 2 and 3.

For each carbonate−isopropylidene−carbonate and isopropylidene−carbonate−isopropylidene triple, a tabulated bond angle potential is used. The latter is obtained from the Boltzmann inversion of the probability density distribution of the corresponding bond angle. The distributions are generated via Metropolis Monte Carlo sampling of a single atomistic chain in a vacuum. The positions of phenylene beads are enforced with a 180° harmonic bond angle potential to avoid introducing of additional torsional degrees of freedom (see ref 6 for details). Finally, the excluded-volume interaction is turned off for beads overlapping due to chemical bonds.

To account for the strong angular dependence of the interaction energy of phenol with nickel the chain-terminating carbonate groups are taken as spheres of the same volume as all other carbonates but with the bond orientations resolved atomistically. The oxygens in the carbonate do not interact via any nonbonded interaction with any other atoms or beads in the system. Their only role is that the orientation of the oxygen−carbonate bond **b**, which defines the orientation of the phenoxy group, is known (see Figure 2).

C. Bead−Wall Interactions. The interaction potential of each bead with the nickel surface is obtained from ab initio calculations, as described in refs 17 and 22. These calculations show that both the carbonate and isopropylidene adsorption energies are much smaller than the characteristic thermal energies in a melt at processing temperature. Below 3.2 Å, both units experience significant repulsion, which is basically independent of their orientation.

On the other hand, the phenolic group is strongly attracted to the surface with the adsorption energy of 1.05 eV ≈ 21 kT at a center-of-mass distance of about 2 Å. This attraction is rather short-ranged (decays below 0.03 eV at a distance 3 Å) and is angular-dependent, with the minimum when the phenol is parallel to the surface. The ab initio calculations suggest that the internal phenylenes, being sterically hindered by the neighboring comonomeric groups, have only weak interaction to the surface. Therefore, in our simulations all internal beads interact with the wall via $10-4$ repulsive potential

$$U_{10-4} = \begin{cases} \epsilon_w\left[\dfrac{2}{5}\left(\dfrac{\sigma_w}{z}\right)^{10} - \left(\dfrac{\sigma_w}{z}\right)^4 + \dfrac{3}{5}\right], & z < \sigma_w \\ 0, & z \geq \sigma_w \end{cases} \quad (1)$$

with $\epsilon_w = 3.77$ kT.

Each chain-terminating phenoxy group i interacts with the array of (111) sites on both walls

$$U_i = \Sigma_j U_s(r_{ij}, \theta_i) \quad (2)$$

where index j runs over the arrays of (111) sites and

$$U_s = \begin{cases} 4\epsilon_i\left[\left(\dfrac{\sigma_i}{r_{ij}}\right)^{12} - \left(\dfrac{\sigma_i}{r_{ij}}\right)^6 + \dfrac{1}{4}\right] - \epsilon(\theta_i), & r_{ij} < r_0 \\ \dfrac{1}{2}\epsilon(\theta_i)\left[\cos\left(\pi\dfrac{r_c - r_{ij}}{r_c - r_0}\right) - 1\right], & r_0 < r_{ij} \leq r_c \\ 0, & r_{ij} \geq r_c \end{cases} \quad (3)$$

where $r_0 = 2^{1/6}\sigma_i = 0.454\sigma = 2$ Å, $r_c = 0.63\sigma = 2.8$ Å is a cutoff distance, $\epsilon_i = 1$ kT, θ_i is the polar angle of the bond linking the outer oxygen of the terminal carbonate and the center of the ith terminal phenoxy, as depicted in Figure 3,

$$\theta_i = \arcsin\left(\dfrac{\mathbf{b}_i \cdot \mathbf{n}}{|\mathbf{b}_i|}\right) \quad (4)$$

Here $\mathbf{n}$ is the surface normal and $\mathbf{b}_i$ is the bond vector. $\epsilon(\theta_i)$ is an empirical function chosen to resemble the situation as given by the ab initio calculations

$$\epsilon(\theta_i) = \epsilon_0 \exp(-\alpha \tan^2 \theta_i) \quad (5)$$

with $\epsilon_0 = 6$ kT. Note that the adsorption energy on the coarse-grained level is significantly lower than given by the ab initio calculations (6 kT instead of 20 kT). This is because each phenoxy bead interacts with an average of three surface atoms simultaneously; moreover, $1-2$ kT of energy is needed to overcome the rotational energy barrier to allow the phenoxy ring to approach a horizontal orientation.

For p-cumylphenolic chain ends we use the adsorption potential of ref 18. In this case the large isopropyledene
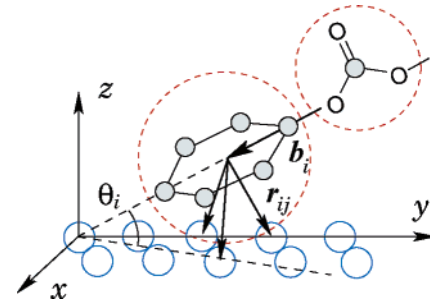

Figure 3. Illustration of the orientation-dependent surface interaction of a terminal phenoxy with the Ni sites in a dual-resolution model. Note that all terminating carbonates are resolved atomistically, so that the angular orientation of the terminating phenolic group is known. The bead corresponding to phenol interacts on average with three Ni sites; the well depth of the interaction potential depends on the tilt angle θ_i.
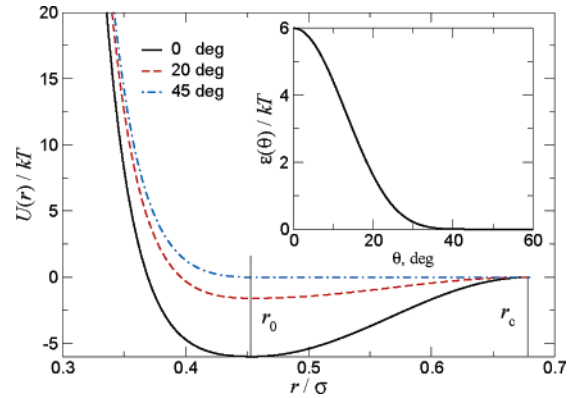

Figure 4. Orientation-dependent potential of the chain-terminating phenoxy group with the sites on the nickel surfaces. Inset illustrates the orientation dependence of the well depth for $\alpha = 10$.
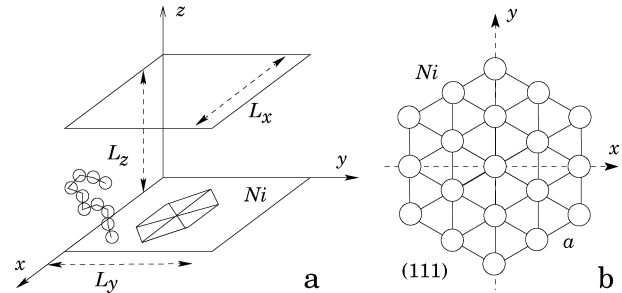

Figure 5. Studied geometry: (a) slit pore of $L_x = 22.23\sigma$ and $L_y = 21.72\sigma$, which corresponds to $n_x = 39$ and $n_y = 22$ unit cells of nickel lattice planes perpendicular to the (111) direction. (b) (111) lattice plane of the face-centered-cubic lattice of nickel. Lattice constant $a = a_{Ni}/\sqrt{2} = 2.51$ Å $= 0.57\sigma$.

group does not allow phenol to approach the wall at the most energetically favorable orientation, resulting in a rather weak attraction (~3.5 kT) of the chain ends to the surface. The parametrization of the potential is described in detail in ref 18.

D. Simulation Details. Polymer melts are confined to a slit pore of thickness L_z (see Table 1) with the walls perpendicular to the z axis, as depicted in Figure 5a. Periodic boundary conditions are employed in x and y directions. The x and y box dimensions are set to $L_x = 22.23\sigma$ and $L_y = 21.72\sigma$, which corresponds to a (111) hexagonal lattice of nickel with 39 and 22 unit cells (see Figure 5). The pore thickness is adjusted in order to achieve bulk number density of beads $n = 0.85$, that is 1.05 g/cm^3, the experimental density at a typical

processing temperature, $T = 570$ K. The units are chosen such that $kT = 1$ with $T = 570$ K, i.e., 1 eV corresponds to about 20 kT; the unit of length is $\sigma = 4.41$ Å.[7]

To generate starting configurations, chains are randomly placed in a box and grown according to the bond length and bond angle distributions. After this, a 5000-step run is performed to remove bead−bead overlaps. During this run, the shifted repulsive Weeks−Chandler−Anderson potential is used with the radial shift decaying linearly from unity to zero; for details, see ref 4. In a second phase, walls are introduced in the system, at a distance 5σ outside the simulation box, and then brought closer during another 5000 steps, until the desired bulk density is reached. Finally, the system is equilibrated until the chains have moved in average a distance equivalent to their radius of gyration.

The production run is performed in NVT ensemble with Langevin thermostat with friction $0.5\tau^{-1}$ and fixed temperature $kT = 1$. The velocity−Verlet algorithm with the time step 0.005τ is used to integrate the equations of motion.

E. Measured Quantities. Simulation results are analyzed to give bead density profiles, center-of-mass density profiles, and the profiles of the orientational ordering of the terminating phenoxy groups. The system is assumed to be invariant with respect to translations in the xy plane. Accordingly, all quantities are averaged over the x and y directions. Accumulation of the simulation averages is done on a grid with the step $\Delta z = L_z/2000$. For a bin i, the number of beads of a particular type, m_i, is calculated. The ensemble average of m_i, normalized by the bin volume $V_b = \Delta z L_x L_y$, results in the bead density profiles (number density vs distance from surface)

$$\rho(z_i) = \frac{\langle m_i \rangle}{V_b} \qquad (6)$$

Adsorption profiles $\gamma(z)$ are calculated from the density profiles as

$$\gamma(z) = \int_{z_0}^{z} [\rho(z') - \rho_b] \, dz' \qquad (7)$$

where ρ_b is the density of the bulk fluid and z_0 is the first bin with the nonzero density. The total adsorption (or coverage) Γ is defined as $\gamma(L_z/2)$, where L_z is the thickness of the slab.

To characterize the angular orientation of the phenolic end group, we calculate two first moments of the angular distribution function of the bond $\mathbf{b}$

$$M_i = \left\langle P_i \left(\frac{\mathbf{n} \cdot \mathbf{b}}{|\mathbf{b}|} \right) \right\rangle \qquad (8)$$

where $i = 1, 2$; $\mathbf{n}$ is a unit vector normal to the surfaces, P_i is the Legendre polynomial of ith order, and $\langle ... \rangle$ denotes the average over all configurations. M_1 gives the average orientation of the bond $\mathbf{b}$. $M_1 = 0$ implies that the distribution function is symmetric with respect to the xy-plane reflection. In this case, M_2 can be used to characterize the distribution: the angular distribution of the vector $\mathbf{b}$ is completely isotropic if $M_2 = 0$; $M_2 = -\frac{1}{2}$ corresponds to the isotropic distribution of the
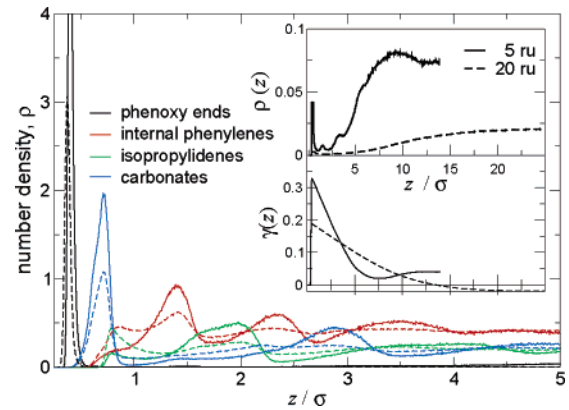

Figure 6. Bead number density profiles for the monodispersed melts of 5 (solid) and 20 (dashed) repeat units. Insets show the chain end density profiles in the vicinity of the wall, $\rho(z)$, and the chain end excess profiles, $\gamma(z)$.

vector $\mathbf{b}$ confined to the xy plane. $S_2 = 1$ means that $\mathbf{b}$ is perpendicular to the xy plane.

III. Results

A. Monodispersed Melts. We first have a look at the bead density profiles of the monodispersed systems of 20 and 5 repeat units. These profiles, shown in Figure 6, have an oscillating structure near the walls, which is typical for any liquid−wall interface and results from packing of the beads at the wall.

Strong attraction of the chain ends to the nickel surface results in a rather sharp peak of the density profiles of the terminating phenylenes at the wall. Its maximum is roughly 2 times larger for the chains of five repeat units, which is a consequence of the increased number of the chain ends in the system. Assuming constant bulk density and Gaussian statistics, we can write $\rho_{bulk} \sim (N/R_z)\rho_{surface}$, where $R_z \sim N^{1/2}$. Therefore, $\rho_{surface} \sim N^{1/2}$, and for the 20:5 mixture we obtain $\rho_{surface}(N=5) = (20/5)^{1/2}\rho_{surface}(N=20)$; i.e., in our case the change in the density of the adsorbed chains ends reflects the initial distribution of the chains in the melt. Of course, one has to remember that, predicting the right tendency, this ratio does not exactly hold for the number of the adsorbed chain ends, reminding us that many mechanisms contribute to the equilibrium chain-end distribution, e.g., conformational entropy of the chains, chain packing next to the wall, bead−wall interactions, etc.

The increase of the number of the adsorbed chain ends is also in agreement with our previous studies of a monodispersed melt with chain length of 10 repeat units (see Figure 13 in ref 7 and Figure 16 in ref 18), the maximum of the adsorption peak for which takes an intermediate value.

The inset of Figure 6 zooms in the chain end density profiles in the vicinity of the wall. The number of the chain ends drops down rather quickly once we move further than 0.5σ from the wall. Moreover, the beads of the adsorbed chains pack better, especially close to the wall, depleting the remaining chains (together with their chain ends) into the bulk. As a result, there is a rather wide region close to the wall where the concentration of the chain ends is much lower than in the bulk. The shorter are the chains, the narrower is this region, basically of the order of the chain end-to-end distance.

The adsorption profiles, $\gamma(z)$, which are also shown in the inset of Figure 6, demonstrate that the total
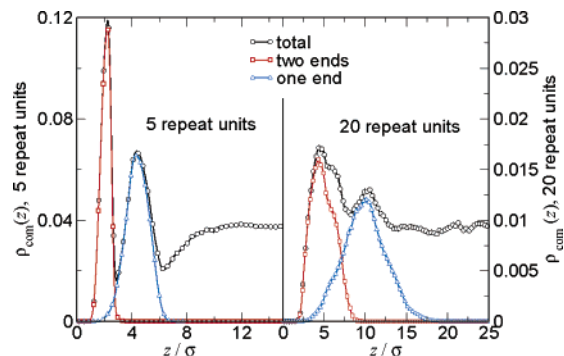
Figure 7. Center-of-mass density profiles for the monodispersed melts of 5 (left) and 20 (right) repeat units. The total amount of chains is divided in two populations: with one end adsorbed on the surface and the both ends adsorbed on the surface. Note the different scales of both the x and y axes.

Figure 8. Chain end density profiles in the vicinity of the wall: (a) minor component; (b) major component. Note different scales for y axes.

Figure 9. Center-of-mass profiles of the major component for the chains adsorbed with both ends.

excess is negative for the chains of 20 repeat units. This implies that the positive contribution to the total excess of a thin, rich in the chain ends layer is smaller than the negative contribution of the wide, poor in chain ends, layer. In fact, this situation would never happen in simple liquids, where the attraction of a particular component to the wall would immediately lead to the surface enrichment and a positive total excess. For the system of five repeat units, however, the total excess becomes positive because of several reasons: first, more chain ends are now adsorbed at the surface; second, the layer from which they are depleted is much thinner.

To asses the probability of end adsorption as a function of distance from the surface we show the center-of-mass density profiles in Figure 7. The total amount of chains is divided in two populations: with only one end adsorbed on the surface and with both ends adsorbed on the surface.

For each component, two layers can be observed, each layer extending for about one radius of gyration. The first layer is formed by the chains with two adsorbed ends, the second comprises of chains adsorbed only with one end. The profiles clearly point out that, in the vicinity of the wall, there is only a small fraction of chains with both free ends; most of the chains are adsorbed with two or at least one end. Moreover, *shorter* chains are more likely to adsorb with two ends than with one end, which can be clearly seen form the difference between the two populations. This trend is similar to the previous results obtained for the melt of 10 repeat units (see Figure 15 in ref 7 and Figure 18 in ref 18).

B. Nonadsorbing and Weakly Adsorbing Chain Ends. For *p*-cumylphenolic chain ends, we found that there is a certain amount of the chain ends localized at the surface as a result of their weak attraction to nickel. However, it is much smaller compared to phenolic chain ends and has little effect on the structure of the melt. We also found that the layering is practically the same as for the nonadsorbing chain ends. The same conclusion can also be made from the center-of-mass density profiles; there is practically no layers formed by the chains with single- and two-end attached chains. As before,[18] these results suggest that the weak adsorption of the *p*-cumylphenolic chain end is responsible only for the local perturbation, while conformational entropy plays the most important role for the structure of the adsorbed layer.

In what follows we therefore concentrate on the systems with strongly adsorbing phenolic chain ends,
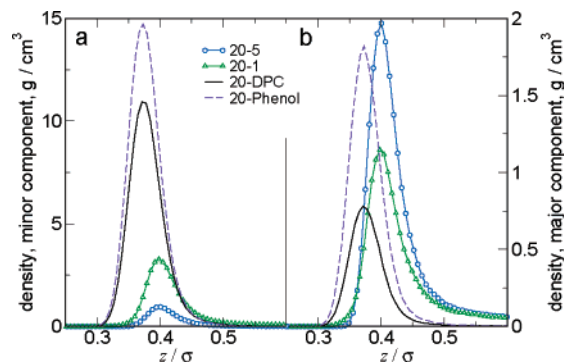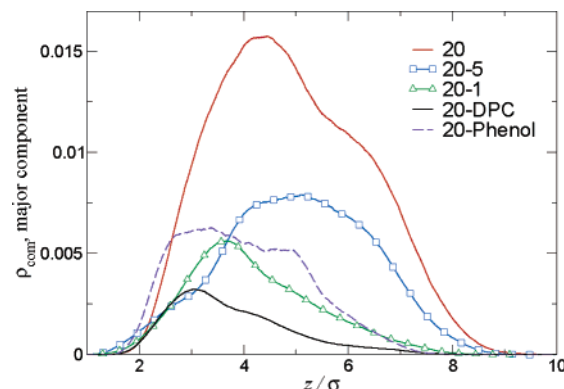
which are also experimentally relevant. The polymer chains in these systems form a well-structured surface layer. We would like to know how the additives change the structure of this layer and how these changes affect the adhesive properties of the melt.

C. Melts with Additives. Let us first have a look at the density profiles of the chain ends of the minor component. These profiles in the vicinity of the wall are shown in Figure 8a. As expected, the contact density of the chain ends of the minor component increases as soon as the chains become shorter due to the increase of the total number of the chain ends in the system. One might anticipate that this increase will result in the reduction of the number of the adsorbed chain ends of the major component, since the surface is already covered by the chains of the minor component. Indeed, the density profiles for the chain ends of the major component, shown in Figure 8b, partially fulfill these expectations: for the 20:5 mixture the number of the chain ends adsorbed at the surface is almost 2 times smaller compared to the monodispersed system and decreases as the chain length decreases. However, in the case of phenol, which has the smallest molecule among the additives, the contact density starts to increase.

Similar trend can be observed from the center-of-mass profiles of the chains adsorbed with two ends, shown in Figure 9. Here the number of the chain ends of the major component (adsorbed with both ends) decreases with the decrease of the chain length of the additive. In the case of phenol, however, the center-of-mass density is again larger than for diphenyl carbonate.

This, at least at a first glance unexpected, increase in the surface coverage of the major component for the phenolic additive is easy to understand if we take into
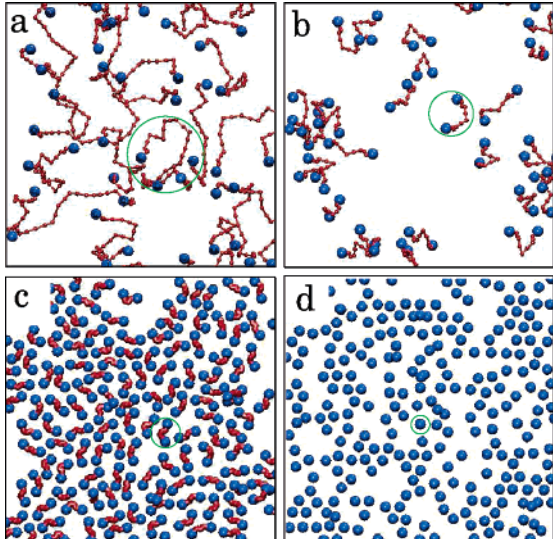
Figure 10. Snapshots of the bidispersed melts: (a) 20:5 repeat units; (b) 20:1; (c) 20:diphenyl carbonate; (d) 20:phenol. Only the molecules of the minor component next to one of the walls are shown. The green circle (shown only as a guide to the eye) depicts the excluded surface area per a molecule adsorbed on the surface.

Table 4. Typical Times Which Are Required To Reach the Stationary Value of the Surface Density of the Adsorbed Chain Ends

N_1, N_2	τ_s ($10^3\tau$)
20, 5	35.4
20, 1	18.1
20, DPC	6.8
20, phenol	6.6

account that the phenol molecule is rather small compared to diphenyl carbonate or one repeat unit BPA-PC. Hence, even though there are more molecules adsorbed on the walls, the net contribution to the screening of the wall−melt interaction is reduced by the smallness of their excluded volume. Indeed, the snapshots of the systems, shown in Figure 10, visualize the competition between the increase of the surface density and decrease of the excluded surface area. Only the molecules of the minor component in the vicinity of the wall (adsorbed layer) are shown. As anticipated, the surface density increases with the decrease of the molecular weight of the molecules. At the same time, the excluded surface area (depicted with a green circle) decreases.

We have also calculated the time dependence of the total amount of the adsorbed chain ends which sheds some light on the dynamics of the chain end adsorption. A fit to empirical equation

$$\rho_s = \rho_s^\infty + (\rho_s^0 - \rho_s^\infty) \exp(-t/\tau_s) \qquad (9)$$

yields the characteristic time τ_s, which tells us when the surface concentration of the adsorbed ends reaches its equilibrium value. Comparing the absolute values (see Table 4), we conclude that the small molecules diffuse and adsorb on the wall much faster than the long ones. Furthermore, this process is also faster than the typical relaxation time of long polymer chains (typical diffusion time of the $N = 20$ chains in the bulk is of the order of $10^4\tau$, see ref 23). In fact, this partially justifies our "quasi-equilibrium" results. (Because of high adsorption energy of 20 kT and limited simulation times, we do not observe desorption of the adsorbed chain ends.)
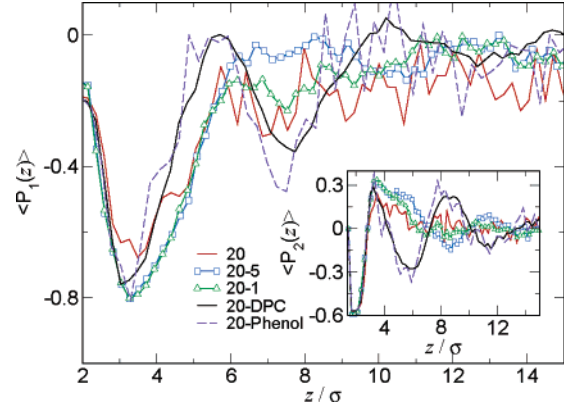

Figure 11. Average orientation, $\langle P_1(z)\rangle$, and the order parameter, $\langle P_2(z)\rangle$, of the terminating bond **b** of the major component.

Finally, we show the average orientation of the terminating bond and the second moment of its angular distribution function in Figure 11. For all mixtures, the average orientation (first moment of the distribution function) is negative, meaning that the bond vector points (on average) toward the wall, since the rest of the chain accommodates itself in the bulk of the cell. The second moment of the angular distribution function has an oscillating structure: it is negative in the vicinity of the wall, reaching the value of -0.5 at the contact. This means that the bond vector is practically perpendicular to the wall normal and has an axially symmetric pancake-like angular distribution function. Away from the wall, the order parameter becomes positive; i.e., the distribution function takes a prolate shape. For shorter chains this modulated structure extends further into the cell bulk, pointing that the orientations of the chain ends of a single molecule are more correlated for the short chains.

IV. Discussion and Conclusions

In conclusion, we have studied adsorption of bidispersed bisphenol A polycarbonate melts on a (111) nickel surface. We find that for monodispersed melts short chains adsorb better than the long ones and the probability for a short chain to adsorb with two ends increases compared to the probability of a single-end adsorption. Both effects stem from the fact that, for the short chains, the number of the chain ends increases and the width of the depleted region next to the wall decreases.

For bidispersed melts, the surface density of the minor component increases with the decrease of its molecular weight. This increase results in the reduction of the number of the attractive surface sites. At the same time, smaller molecules occupy less surface area. The competition between two mechanisms selects diphenyl carbonate as the additive providing the most efficient screening of the interaction between the polycarbonate melt and the nickel surface.

We now turn a brief discussion on the implications of this work. As we have already mentioned in introduction, polycarbonate processing involves its fast shearing past metal surfaces. At this stage both the bulk viscosity and the hydrodynamic boundary conditions, quantified by the slip length and the friction coefficient, are important.

Boundary conditions are, of course, extremely sensitive to the structure of the adsorbed layer.[24−26] In fact,

there are two mechanisms contributing to the boundary conditions:[19] the first one is due to scattering of the adsorbed parts of chains on the surface potential. This potential induces the local density and the chain conformation modulation in the adsorbed layer, and energy is lost from these modulations through the coupling to the thermostat (or through the walls in a real system), similar to the situation observed in any adsorbed surface layers.[27] In our particular situation, small molecules adsorbed on the surface will serve as additional obstacles which the chain ends of the long chains have to overcome while slipping over the surface. As a result, the slip length (the distance behind the wall at which the velocity profile extrapolates to zero) will decrease and stick boundary conditions will settle in the system. On the other hand, polymer brushes made of single-end-grafted chains undergo a coil/stretch transition and disentangle from the melt at a given shear rate, which depends on the surface concentration of the grafted chains.[28,29] In our case additives reduce the surface concentration of the one-end-adsorbed chains entangled with the melt and, therefore, favor the slip boundary condition, even for small shear rates.

Competition of the above mechanisms will most probably result in a nontrivial friction law, with both the slip length and the friction force depending on the shear rate and the molecular weight of the additive. This work is in progress.[30]

References and Notes

(1) Morbitzer, L.; Grigo, U. *Angew. Makromol. Chem.* **1988**, *162*, 87−107.
(2) DeRudder, J. L. *Handbook of Polycarbonate Science and Technology*; Marcel Dekker: New York, 2000.
(3) Tsai, S. F.; Lan, I. K.; Chen, C. L. *Comput. Theor. Polym. Sci.* **1998**, *8*, 283−289.
(4) Tschop, W.; Kremer, K.; Batoulis, J.; Burger, T.; Hahn, O. *Acta Polym.* **1998**, *49*, 61−74.
(5) Tschop, W.; Kremer, K.; Hahn, O.; Batoulis, J.; Burger, T. *Acta Polym.* **1998**, *49*, 75−79.
(6) Abrams, C. F.; Kremer, K. *Macromolecules* **2003**, *36*, 260−267.
(7) Abrams, C. F.; Delle Site, L.; Kremer, K. *Phys. Rev. E* **2003**, *67*, 021807.
(8) Baschnagel, J.; Binder, K.; Doruker, P.; Gusev, A. A.; Hahn, O.; Kremer, K.; Mattice, W. L.; Muller-Plathe, F.; Murat, M.; Paul, W.; Santos, S.; Suter, U. W.; Tries, V. *Adv. Polym. Sci.* **2000**, *152*, 41−156.
(9) Kremer, K. *Macromol. Chem. Phys.* **2003**, *204*, 257−264.
(10) Namhata, S.; Guest, M. J.; Aerts, L. M. *J. Appl. Polym. Sci.* **1999**, *71*, 311−318.
(11) Aubouy, M.; Guiselin, O.; Raphael, E. *Macromolecules* **1996**, *29*, 7261.
(12) Aubouy, M. *Phys. Rev. E* **1997**, *56*, 3370−3377.
(13) Manghi, M.; Aubouy, M. *Phys. Rev. E* **2003**, *68*, 041802.
(14) Smith, K. A.; Vladkov, M.; Barrat, J. L. *Macromolecules* **2005**, *38*, 571−580.
(15) Swalen, J. D.; Allara, D. L.; Andrade, J. D.; Chandross, E. A.; Garoff, S.; Israelachvili, J.; McCarthy, T. J.; Murray, R.; Pease, R. F.; Rabolt, J. F.; Wynne, K. J.; Yu, H. *Langmuir* **1987**, *3*, 932−950.
(16) Claesson, P. M.; Ederth, T.; Bergeron, V.; Rutland, M. W. *Adv. Colloid Interface Sci.* **1996**, *67*, 119−183.
(17) Delle Site, L.; Abrams, C. F.; Alavi, A.; Kremer, K. *Phys. Rev. Lett.* **2002**, *89*, 156103.
(18) Delle Site, L.; Leon, S.; Kremer, K. *J. Am. Chem. Soc.* **2004**, *126*, 2944−2955.
(19) Zhou, X.; Andrienko, D.; Delle Site, L.; Kremer, K. *Europhys. Lett.* **2005**, *70*, 264−270.
(20) Cheah, K.; Cook, W. D. *Polym. Eng. Sci.* **2003**, *43*, 1727−1739.
(21) Tuinier, R.; Taniguchi, T. *J. Phys.: Condens. Matter* **2005**, *17*, L9-L14.
(22) Delle Site, L.; Alavi, A.; Abrams, C. F. *Phys. Rev. B* **2003**, *67*, 193406.
(23) Leon, S.; Delle Site, L.; Kremer, K. *Macromolecules*, in press.
(24) Léger, L.; Raphaël, E.; Hervet, H. *Adv. Polym. Sci.* **1999**, *138*, 185−225.
(25) Grest, G. S. *Adv. Polym. Sci.* **1999**, *138*, 149.
(26) Klein, J. *Annu. Rev. Mater. Sci.* **1996**, *26*, 581−612.
(27) Cieplak, M.; Smith, E. D.; Robbins, M. O. *Science* **1994**, *265*, 1209.
(28) Brochard, F.; de Gennes, P. G. *Langmuir* **1992**, *8*, 3033.
(29) Ajdari, A.; Brochard-Wyart, F.; de Gennes, P. G.; Leibler, L.; Viovy, J. L.; Rubinstein, M. *Physica A* **1994**, *204*, 17.
(30) Zhou, X.; Andrienko, D.; Kremer, K. *J. Chem. Phys.*, in press.

MA0506029